Dental Materials 40 (2024) 1171–1183

Contents lists available at ScienceDirect

Dental Materials

journal homepage: www.elsevier.com/locate/dental

Mechanical and physical properties of splint materials for oral appliances produced by additive, subtractive and conventional manufacturing

Tina Maleki [a,*], John Meinen [a], Andrea Coldea [a], Marcel Reymus [b], Daniel Edelhoff [a], Bogna Stawarczyk [a]

[a] Department of Prosthetic Dentistry, University Hospital, LMU Munich, Munich, Germany
[b] Department of Conservative Dentistry and Peridontology, University Hospital, LMU Munich, Munich, Germany

ARTICLE INFO

Keywords:
Splints
3D-printing
Flexural strength
Elastic modulus
Martens hardness
Water sorption
Water solubility
Degree of conversion

ABSTRACT

Objectives: To investigate the flexural strength (FS), elastic modulus (E), Martens hardness (HM), water sorption (w_{sp}), water solubility (w_{sl}) and degree of conversion (DC) of 3D-printed, milled and injection molded splint materials.

Methods: Specimens (N = 1140) were fabricated from five 3D-printed (GR-22 flex, GR-10 guide, ProArt Print Splint clear, V-Print Splint, V-Print Splint comfort), five milled (BioniCut, EldyPlus, ProArt CAD Splint clear, Temp Premium Flexible, Thermeo) and two injection molded (PalaXPress clear, Pro Base Cold) materials. FS, E, HM, w_{sp}, w_{sl} and DC were tested initially (24 h, 37 °C, H_2O), after water storage (90 d, 37 °C, H_2O) as well as after thermal cycling (5000 thermal cycles, 5/55 °C). Data were analyzed with Kolmogorov-Smirnov, Kruskal-Wallis, Mann-Whitney U test and Spearman's correlation ($p < 0.05$).

Results: Initially, the mean flexural strength values ranged from 1.9 to 90.7 MPa for printed, 3.8 to 107 MPa for milled and 99.7 to 102 MPa for injection molded materials. The initial mean elastic modulus values were 0.0 to 2.4 GPa for printed, 0.1 to 2.7 GPa for milled and 2.8 GPa for injection molded materials. The initial mean Martens hardness values were 14.5 to 126 N/mm^2 for printed, 50.2 to 171 N/mm^2 for milled and 143 to 151 N/mm^2 for injection molded materials. Initially, the mean water sorption values ranged from 23.1 to 41.2 µg/mm^3 for printed, 4.5 to 23.5 µg/mm^3 for milled and from 22.5 to 23.3 µg/ mm^3 for injection molded materials. The initial mean water solubility values ranged from 2.2 to 7.1 µg/mm^3 for printed, 0.0 to 0.5 µg/mm^3 for milled and 0.1 to 0.3 µg/mm^3 for injection molded materials. After water storage and thermal cycling most of the values decreased and some increased. The mean DC values ranged initially from 72.3 to 94.5 %, after water storage from 74.2 to 96.8 % and after thermal cycling from 75.6 to 95.4 % for the printed materials.

Significance: The mechanical and physical properties of printed, milled and injection molded materials for occlusal devices vary and are influenced by aging processes. For clinical applications, materials need to be chosen according to the specific indications.

1. Introduction

The use of occlusal devices in dentistry is diverse and covers a wide range of areas. They are used as sports guards, snoring splints, medication carriers (e.g., bleaching splints) or to treat fractures in maxillofacial surgery. In orthodontics teeth and jaw malposition are corrected and in prosthodontics removable bite splints are used to test a new bite position. The most common clinical application however is the treatment of bruxism and craniomandibular dysfunction. In addition to pharmacological measures (injection of botulinum toxin), psychotherapy and physiotherapy, occlusal splints serve as a reliable dental therapy to reduce bruxism [1] and protect tooth structure from excessive wear [2]. Splints can be modeled from wax, embedded in flasks, and then injected with an auto- or hot-polymerizing liquid powder polymethyl methacrylate (PMMA) [3]. This differs from splints fabricated by thermoforming, often from polyethylene (PET-G), which are occlusally customized with polymethylmethacrylate [4]. The layered scattering of splints represents the third alternative of the conventional technique. Although this method has proven itself for decades, it has disadvantages such as residual monomer content, polymerization

* Corresponding author.
E-mail address: Tina.Maleki@med.uni-muenchen.de (T. Maleki).

https://doi.org/10.1016/j.dental.2024.05.030
Received 25 September 2023; Received in revised form 15 March 2024; Accepted 29 May 2024
Available online 8 June 2024

shrinkage, susceptibility to errors when mixing the resin, high time requirement and high laboratory costs [5]. Computer-aided design (CAD) and computer-aided manufacturing (CAM) in dentistry enable the fabrication of splints by subtractive milling or additive 3D-printing. The easy availability of patient-specific data and the rapid fabrication of reproducible splints in case of fracture or loss are advantages over the conventional manufacturing process [6]. In the subtractive approach, the high conversion rate of the double bonds of the industrially manufactured polymer-based blanks leads to a better fit by passing the polymerization shrinkage that has already occurred during the fabrication of the blank [7]. A maximum of two splints can be inserted into one blank, resulting in high material consumption and thus high costs. In the subtractive milling process, up to 90 % is residue [8]. Therefore, the additive manufacturing process is becoming increasingly important in dentistry. Printing complex geometries, saving time by placing multiple restorations on the build platform, and lower material consumption open new possibilities. Digital Light Projection (DLP) technology is currently the primary method for printing dental splints. The speed of the printing process is independent of the number of objects placed and higher than in the SLA (Stereolithography) process [9].

Studies show higher mechanical properties of injection molded and milled materials compared to 3D-printed materials [5–7,10–13]. However, the printing angle can influence the properties. While higher hardness and lower surface roughness have been studied in 3D-printed materials at 45° printing angle [11], 0° printing angle shows the highest wear resistance, followed by 45° and 90° [12]. Post-polymerization also influences hardness due to the correlation of hardness and conversion rate [14,15]. Since splints can fracture in routine use because of stresses, for example during insertion and removal or due to high chewing forces while grinding, the mechanical properties are of high importance. The hardness of a material is an important parameter as it characterizes the behavior of the elastic-plastic surface and it allows to draw conclusions about the surface degradation induced by aging [16,17]. By measuring the flexural strength, information about the resistance of a material to fracture during force application and its resistance against crack propagation can be obtained, while the elastic modulus characterizes the stiffness and rigidity [10]. Studies have shown that especially 3D-printed materials show a decrease in mechanical properties after water storage [15]. The correlation between mechanical properties and the water sorption and solubility should therefore be further investigated. The purpose of this in vitro study was to evaluate the effect of the material and artificial aging on flexural strength, elastic modulus, Martens hardness, water sorption and solubility as well as conversion rate to identify the opportunities and the limitations of different occlusal device materials. The tested null hypotheses were as follows: a) material and b) aging have no effect on the mechanical and chemical properties tested in this investigation.

2. Materials and methods

The properties of five additive, five subtractive and two conventional manufactured splint materials were examined (Fig. 1, Table 1). Flexural strength and elastic modulus (N = 540, n = 45/material), Martens hardness (N = 240, n = 20/material), water sorption and solubility (N = 360, n = 30/material) and the conversion rate (only additively manufactured specimens; N = 150, n = 30/material) of the splint materials were tested.

2.1. Specimen preparation

2.1.1. Additive manufactured specimens

The specimen's geometry was designed (64.2 ×10.2 ×3.5 mm, 5 ×10×25 mm, 50 ×0.5 mm) (stl- master data sets; Autodesk meshmixer, ADSK Ireland Ltd.) and additively manufactured using Digital Light Processing (D20II, RapidShape, Heimsheim, Germany; PrograPrint PR5, Ivoclar Vivadent, Schaan, Liechtenstein) (Table 2). The specimens were placed perpendicular to the build platform with supporting structures (Autodesk Netfabb 2022.0, ADSK Ireland Ltd.) (Fig. 2). The post-processing steps were performed according to the manufacturer's instructions (Table 2).

2.1.2. Subtractive manufactured specimens

The specimens for flexural strength and elastic modulus measurements (64.2 ×20.5 ×3.6 mm) were nested (Ceramill Mind, Amann-Girrbach, Koblach, Austria) and milled (Ceramill Motion II, Amann-Girrbach). The connectors were removed, and the panels were halved along the length. The Martens hardness specimens were cut out of the blank with a low-speed water-cooled diamond saw (Secotom 50, B0D20,

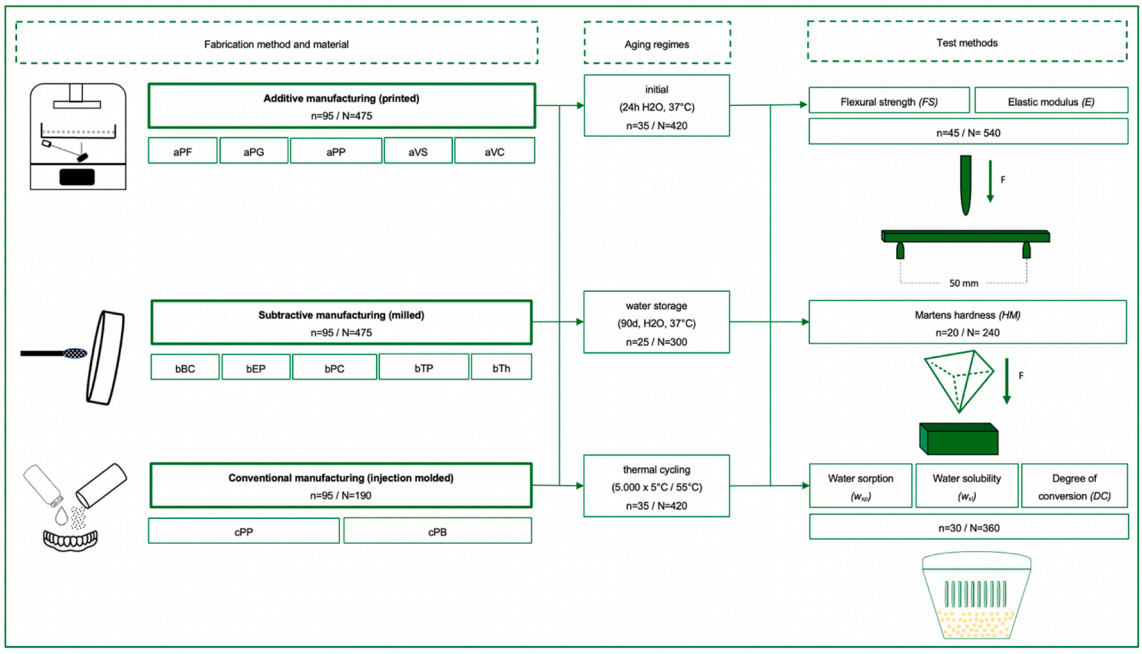

Fig. 1. Study design.

Table 1
The manufacturing types, abbreviations, materials, manufacturers, compositions, and lot numbers (Lot No.) of tested materials.

Manufacturing type	Abbreviation	Material	Manufacturer	Composition	Concentration %	Lot No.
Printed	aPF	GR-22 flex	pro3dure medical, Iserlohn, Germany	Oligomers; methacrylic resins, multifunctional	< 75	201220217
				Methacrylic resins, monofunctional	> 25	
				Photoinitiators (various);	< 2 (in total)	
				Pigments/stabilizers	n.g.	
	aPG	GR-10 guide		Esterification products of 4,4′-isopropylidenediphenol, ethoxylated and 2-methylprop-2-enoic acid	80-100	030220221
				Diphenyl (2,4,6- trimethylbenzoyl) phosphine oxide	< 03	
	aPP	ProArt Print Splint clear	Ivoclar Vivadent, Schaan, Liechtenstein	Urethane acrylate oligomer	n.g.	Z02PY5
				Triethylene glycol dimethacrylate		
				Urethandimethacrylat (UDMA)		
				Bis-Glycidyldimethacrylat (BisGMA)		
				Diphenyl(2,4,6-trimethylbenzoyl) phosphine oxide		
	aVS	V-Print Splint	VOCO, Cuxhaven, Germany	Polyesterdimethacrylate	50-100	2202641
				ethoxylated bisphenol-A dimethacrylate (Bis-EMA)	25-50	
				Triethylene glycol dimethacrylate	5-10	
				Hydroxypropylmethacrylate	5-10	
				Diphenyl (2,4,6-trimethylbenzoyl) phosphine oxide	≤ 2.5	
				Butylated hydroxytoluene (BHT)	≤ 2.5	
	aVC	V-Print Splint comfort		Aliphatic acrylate	25-50	2209436
				Triethylene glycol dimethacrylate	5-10	
				Diphenyl(2,4,6-trimethylbenzoyl) phosphine oxide	≤ 2.5	
Milled	bBC	BioniCut	Bredent, Senden, Germany	Polyoxymethylen (POM -C); pigments	n.g.	513005 (height 20) 523543 (height 25)
	bEP	EldyPlus	DentalPlus, Samerberg, Germany	Polyethylenterephthalat (PET-G); Glykol; Ethanol	n.g.	21ELGK26
	bPC	ProArt CAD Splint clear	Ivoclar Vivadent	Polymethylmethacrylate (PMMA)	> 99	YB3KR3
	bTP	Temp Premium Flexible	Zirkonzahn, South Tyrol, Italy	Thermoplastic polycarbonate (PC)	n.g.	16261
	bTH	Thermeo	pro3dure medical	Polyethylmethacrylat, homopolymer	> 90	240120221
				1,2- Cyclohexandicarbonsäurediisononylester	< 10	
Injection molded	cPP	PalaXPress clear	Kulzer, Hanau, Germany	Powder	> 95	M010121 (powder)
				Methacrylate copolymers1-benzyl-5-phenylbarbituric acid	< 5	M010262 (liquid)
				Liquid	> 90	
				Methacrylate monomer	5-10	
				1,4-butanediol dimethacrylate	< 1	
				Trioctylmethylammoniumchlorid		
	cPB	Pro Base Cold	Ivoclar Vivadent	Powder	< 95	YB380P (powder)
				Polymethylmethacrylate (PMMA) dibenzoyl peroxide	1-2.5	Z032DH (liquid)
				Liquid	60-100	
				Methyl methacrylate 1,4-butanediol dimethacrylate	3-5	

Struers, Ballerup, Denmark) (disk speed 2200 rpm, feed rate 0.070 mm/s). For water sorption and solubility specimens, a cylinder (50 mm diameter) was milled (Ceramill Motion II) and cut with a low-speed water-cooled diamond saw (Secotom 50, B0D20, Struers) into 0.5 mm thick slices (bBC, bEP, bPC, bTP: 2200 rpm, 0.060 mm/s; bTH: 2200 rpm, 0.030 mm/s) (Fig. 3).

Therefore, a cube shaped holder was printed (ProArt Print Splint clear, Ivoclar Vivadent) and fixed (UHU Plus Endfest 2-K-Epoxidkleber, UHU, Bühl, Germany).

2.1.3. Conventionally manufactured specimens

The specimens were manufactured using the injection technique (Fig. 4). For this purpose, the stl master data sets were used to print specimens (ProArt Print Splint clear, Ivoclar Vivadent) and embed them with plaster (pico-crema soft, picodent, Wipperfürth, Germany) in a flask (Palajet Duoflask, Kulzer, Hanau, Germany). Casting channels made of wax (PalaXpress accessories Sprue wax, Kulzer) were applied. A silicone conter (Fifty-Fifty 95 putty, Klasse 4 dental, Augsburg, Germany) was used to allow the removal of the embedded specimens from the plaster and the final layer of plaster conter was applied. The wax was scalded and the flask with the desired cavity was isolated twice (Aislar, Kulzer). The cuvette was clamped in a compressed air injection unit (Palajet, Kulzer) and the material was injected. The recommended mixing ratio of each material was used according to the manufacturer's instructions. The cuvette remains in the injection device for 7 min. The final polymerization was performed for 35 min in a pressure pot (two bar, 55 °C) (Palamat elite, Kulzer).

For flexural strength and elastic modulus measurements, specimen plates with dimensions 65.0 × 40.0 × 5.0 mm were injected [ISO 20795-1: 2013] and cut lengthwise with a low-speed water-cooled diamond saw (Secotom 50, B0D20, Struers) (2200 rpm, 0.070 mm/s). For Martens hardness, specimens with final geometries were embedded in the flask (Fig. 4). For water sorption and solubility, a hollow cylindrical shape (50 mm diameter) was created in a flask and injected. The cylinder was cut with a low-speed water-cooled diamond saw (Secotom 50, B0D20, Struers) into the desired slices with a thickness of 0.5 mm (cPP, cPB: 2200 rpm, 0.050 mm/s) (Fig. 3B). Therefore, a cube shaped holder was printed (ProArt Print Splint clear, Ivoclar Vivadent) and fixed (UHU Plus Endfest 2-K-Epoxidkleber, UHU).

2.1.4. Specimen finishing

All flexural strength/elastic modulus (N = 540; 64.0 ×10.0 ×3.3 ± 0.2 mm) and Martens hardness (n = 240; 5.0 ×10.0 ×25.0 mm) specimens were wet-ground (Abramin, Struers) to their final dimension using silicon carbide paper (SiC Foil P1200, Struers) and water irrigation [ISO 20795-1:2013]. Due to the saw blade graining and motion under water

Table 2
The post-processing of the printed materials tested.

Material	DLP 3D-printer	Cleaning	Postpolymerization
aPF	D20II, RapidShape, Heimsheim Germany	10 min in Isopropanol (IPA) ≥ 97 % (SAV LP, Flintsbach, Germany) in an ultrasonic bath (Sonorex Super RK1022; Bandelin electronic, Berlin, Germany)	2 × 750 flashes (Otoflash G171, NK-Optik)
aPG		4 min in IPA ≥ 97 % % (SAV LP) in an ultrasonic bath (Sonorex Super RK1022; Bandelin electronic)	2 × 1000 flashes (Otoflash G171, NK-Optik, Baierbrunn, Germany)
aPP	PrograPrint PR5, Ivoclar Vivadent, Schaan, Liechtenstein	10 min pre-cleaning 5 min cleaning in IPA ≥ 97 % (SAV LP) in PrograPrint Clean (Ivoclar Vivadent)	90 s in PrograPrint Cure (Ivoclar Vivadent)
aVS	D20II, RapidShape	3 min pre-cleaning 2 min cleaning in IPA ≥ 97 % (SAV LP) in an ultrasonic bath (Sonorex Super RK1022; Bandelin electronic)	1 × 2000 flashes 2 min cooling 1 × 2000 flashes (Otoflash G171, NK-Optik)
aVC		5 min pre-cleaning 3 min cleaning in IPA ≥ 97 % (SAV LP) in an ultrasonic bath (Sonorex Super RK1022; Bandelin electronic)	1 × 2000 flashes 2 min cooling 1 × 2000 flashes (Otoflash G171, NK-Optik)

Fig. 2. Additive manufactured specimens.

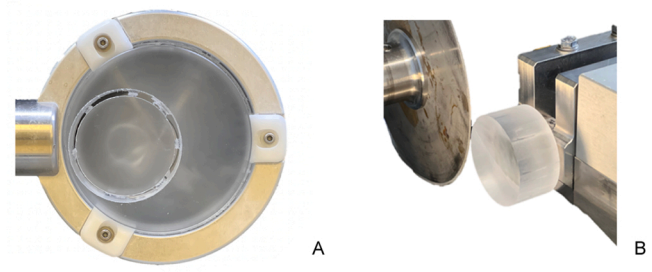

Fig. 3. Specimen preparation. A, Milled cylinder for water sorption and solubility. B, Cutting a cylinder with a cube shape holder.

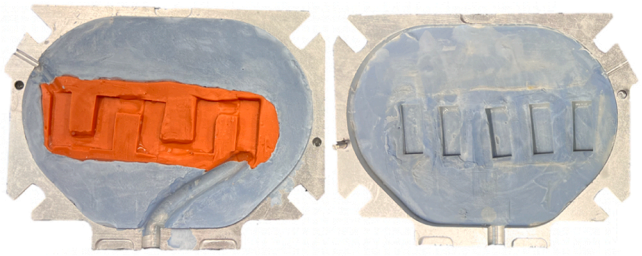

Fig. 4. Injection technique; Martens hardness specimen geometry embedded in a flask.

irrigation, the specimens for water sorption and solubility were cut to their final dimensions 50.0 × 50.0 × 0.5 mm [ISO 20795-1:2013] without the need for additional grinding.

2.2. Aging regime

All measurements were performed after three different aging subgroups.

1) Initial: storage in 37 °C deionized water (HERAcell 150, Thermo Fisher Scientific, Waltham, USA) for 24 h
2) Water storage: storage in 37 °C deionized water (HERAcell 150) for 90 d
3) Thermal cycling: 5000 thermal cycles with an immersion time of 30 s in 5 °C/55 °C deionized water and a dwell time of 5 s (THE-1100, SD Mechatronik, Feldkirchen-Westerham, Germany)

After initial storage and the initial measurement, the same HM specimens were stored in water for further 89 days (water storage group).

2.3. Test methods

The **three-point bending test was performed** at room temperature (23 °C) using a universal testing machine (Zwick/Roell 1445 RetroLine, ZwickRoell, Ulm, Germany) with a crosshead speed of 5 mm/min and a load cell with a capacity of 500 N [ISO 20795-1]. The distance between the specimen's supports was 50 mm. The measurement was considered finished when a maximum deformation of 10 mm was reached. Flexural strength was calculated from the load at fracture or at maximum deformation. Flexural strength and elastic modulus values were obtained according to the following formulas: $FS = 3 *F*l/2 *b*h^2$; $E = [F_1 *l^3/4 *b*h^3 *d]/1000$, where FS is the flexural strength (MPa), F is the maximum force (N) applied to the specimen, l is the support span (mm), b is the specimen width (mm), h is the specimen height (mm), E is the elastic modulus (GPa), F_1 is the load (N) at a point in the straight line portion of the load/deflection curve, and d is the recorded deflection (mm) at load F_1.

A Martens hardness testing machine (ZHU 0.2/ Z2.5, Zwick Roell) was used to determine the **Martens hardness**. The surface of the specimens was indented by a Vickers diamond indenter with a force of 9.81 N. Three measurements were performed on each specimen and HM was automatically calculated with the corresponding software (testXpert V12.3 Master, Zwick Roell). The following equation was used to compute HM: $HM = F/A_s(h)$, where HM is the Martens hardness (N/mm^2), F is the maximum test load (N) and $A_S(h)$ is the area of the indenter penetrating the surface at the distance h (mm^2).

The **water sorption and solubility** specimens were placed in a desiccator, containing freshly dried silica gel and were stored in an oven (Modell 100–800, Memmert, Schwabach, Germany) at 37 °C for 23 h. Subsequently, the specimens were directly transferred to the second desiccator at 23 °C with freshly dried silica gel for 60 min and then

weighed (NewClassic MF, Mettler-Toledo, Greifensee, Switzerland). The cycle described was repeated until the mass loss of each specimen between successive weighing operations did not exceed 0.2 mg (conditioned mass m_1) [ISO 20795-1:2013]. At that point the volume (V) for each specimen was calculated from the average over three measurements of the diameter and from the average over five measurements of the thickness. The conditioned specimens were either stored in water for 24 h, 90 days or were thermal cycled. The specimen discs were then removed from the water, dried and weighed 60 s after removal (m_2). The specimens were then reconditioned to a constant mass (reconditioned mass m_3) in the desiccator. The value for w_{sp} and w_{sl} was calculated for each specimen using the following equation: $w_{sp} = [m_2 - m_3]/V$; $w_{sl} = [m_1 - m_3]/V$, where w_{sp} is the water sorption (μg/mm^3), w_{sl} is the water solubility (μg/mm^3), m_1 is the mass of the dried specimen (μg), m_2 is the mass of the specimen after aging (μg) and m_3 is the mass of the specimen after second drying cycle (μg).

The **conversion rate** was determined for all additive manufactured materials using a Raman spectrophotometer (inVia Qontor, Renishaw, New Mills, UK). The Raman spectra of the liquid unpolymerized printing materials was initially measured ten times to obtain an average value ($R_{unpolymerized}$). After each aging, the Raman spectra of the polymerized printed materials was determined ($R_{polymerized}$). The measurements were performed at a wavelength of 785 nm with 100 % laser power. The height values of the peaks at 1610 cm^{-1} and 1640 cm^{-1} were determined by the curve fit function with the WiRE 4.4 software (Renishaw). If the curves were too small for a successful fit, the height value was read manually. The conversion rate was calculated from the following formula: $DC = 100 \times [1 - (R_{poly}/R_{unpoly})]$, where DC is the conversion rate and R is the height at 1610 cm^{-1}/height at 1640 cm^{-1}.

2.4. Statistical analysis

The data were analyzed using descriptive analysis followed by Kolmogorov–Smirnov to test the violation of normal distribution. Non-parametric tests were performed, as 19,4 % (7/36) of the FS, 25,0 % (9/36) of the E, 22,2 % (8/36) of the HM, 5,5 % (2/36) of the w_{sp}, 13,8 % (5/36) of the w_{sl}, and 13,3 % (2/15) of the DC groups deviated from normal distribution. Kruskal–Wallis test and Mann-Whitney-U test were computed to determine significant differences between the different materials and aging regimes. Spearman's correlation was used to test the association between FS, HM, w_{sp}, w_{sl} and DC. The data was analyzed with SPSS version 29.0 (IBM, SPSS, Statistics, Armonk, NY, USA). Statistical significance was inferred when p-values < 0.05.

3. Results

3.1. Comparison of flexural strength of all tested materials

3.1.1. Impact of the material on flexural strength

Within the initial group significant differences were observed for all materials, except bPC and bTP (p = 0.694) (Table 3, Fig. 5). aPF showed initially the lowest FS values compared to the remaining materials, followed by bTH, aVC, aPG, aPP, bEP, bBC, aVS, cPP and cPB (p < 0.001–0.021), while bPC and bTP presented the highest FS values regardless the aging regime.

Within the water storage group also aPF showed the lowest FS values compared to the remaining materials, followed by bTH, aVC, aPP, aPG, cPP and bEP (p < 0.001–0.012). aVS showed lower values than bBC, bPC and bTP after water storage (p < 0.001). cPB and bBC revealed lower values compared to bPC and bTP within the water storage group (p < 0.001).

Within the thermal cycling group also aPF presented the lowest FS values compared to all materials, followed by bTH (p < 0.001). aPG and aVC showed lower FS values than aPP, bEP, aVS, cPP, bBC, cPB, bPC and bTP (p < 0.001). aPP showed lower FS values than bEP, aVS, cPP, bBC, cPB, bPC and bTP after thermal cycling (p < 0.001). bEP presented lower values than aVS, cPP, bBC, cPB, bPC and bTP after thermal cycling (p < 0.001), while aVS revealed lower values compared to bBC, cPB, bPC and bTP (p < 0.001–0.006). cPP, bBC, cPB showed lower FS values within the thermal cycling group compared to bPC and bTP (p < 0.001).

The load-deflection curves (Fig. 11) represent that during the 3-point bending test, only aVS, bPC and the injection molded specimen fractured.

3.1.2. Impact of artificial aging on flexural strength

Artificial aging significantly affected the FS values of the materials except for bPC and bEP (p = 0.161–0.237) (Table 3, Fig. 5). The highest FS values were obtained in the initial group for aPG, aPP, aVS, cPP and cPB compared to the other aging regimes (p < 0.001–0.003). aPP, cPP and cPB showed higher values after thermal cycling compared to water storage (p < 0.001–0.006). Interestingly thermal cycling increased the FS values for aPF, aVC, bTP, bBC and bTH compared to the initial group (p < 0.001–0.017). The FS values were higher after water storage compared to the initial group for aVC, bBC and bTH (p < 0.001–0.024).

3.2. Comparison of elastic modulus of all tested materials

3.2.1. Impact of the material on elastic modulus

Within the initial group significant differences were observed for all materials, except bPC, cPP and cPB (p = 0.350–0.724) (Table 3, Fig. 6). aPF showed initially the lowest E values compared to the remaining materials, followed by bTH, aVC, aPG, bEP, aPP, bTP, aVS and bBC (p < 0.001–0.048), while bPC, cPP and cPB presented the highest E values.

After water storage, also aPF presented the lowest E values compared to all materials, followed by bTH (p < 0.001). aPP showed lower E values than aPG, bEP, bTP, aVS, cPB, bBC, cPP and bPC (p < 0.001–0.027). aVC and aPG showed lower values compared to the remaining materials (p < 0.001), followed by bEP, bTP, aVS, cPB, bBC, cPP and bPC (p < 0.001–0.022).

Within the thermal cycling group also aPF presented the lowest E values compared to all materials, followed by bTH (p < 0.001). aPG and aVC showed lower E values compared to the remaining materials, followed by aPP and bEP (p < 0.001). aVS and bTP presented lower values compared to the remaining materials, followed bBC, cPB, cPP and bPC (p < 0.001–0.002).

3.2.2. Impact of artificial aging on elastic modulus

Artificial aging significantly affected the E values of the materials (Table 3, Fig. 6). The highest values were obtained in the initial group for aPP, aVS and cPB compared to the other aging regimes (p < 0.001–0.013), while aPP and cPB showed significantly higher values after thermal cycling than after water storage (p < 0.001). The highest E values were calculated in the initial and thermal cycling group for aPG and bTP (p < 0.001). aPF, aVC, bBC, bPC and cPP showed the highest E values after thermal cycling compared to the other aging regimes (p < 0.001–0.048), while aVC and bBC and bEP showed higher values after water storage compared to the initial group (p = 0.004–0.042) and cPP showed lower values after water storage compared to the initial group (p = 0.001). The highest E values were calculated in the thermal cycling and water storage group for bTH (p < 0.001).

3.3. Comparison of Martens hardness of all tested materials

3.3.1. Impact of the material on Martens hardness

Within the initial group aPF showed the lowest HM values followed by aVC, bTH, aPG, bEP and aPP compared to the remaining materials (p < 0.001–0.001) (Table 3, Fig. 7). bTP, bBC and aVS presented lower HM values compared to cPB, cPP and bPC (p < 0.001–0.009). cPB and cPP showed lower values than bPC (p < 0.001–0.002).

After water storage, aPF revealed the lowest HM values compared to

Table 3
Descriptive statistics (mean, standard deviation (SD) and 95 % confidence intervals (CI)) for *FS* (MPa), *E* (GPa), *HM* (N/mm^2), w_{sp} (μg/mm^3), w_{sl} (μg/mm^3), DC of the different groups.

Material	Aging	FS		E		HM		w_{sp}		w_{sl}		DC	
		Mean ± SD	95 % CI	Mean ± SD	95 % CI	Mean ± SD	95 % CI	Mean ± SD	95 % CI	Mean ± SD	95 % CI	Mean ± SD	95 % CI
aPF	Initial	1.9 ± 0.4^{aA}	[1.6;2.3]	0.0 ± 0.0^{aA}	[0.0;0.2]	14.5 ± 2.7^{aA}	[11;17]	38.5 ± 4.1^{hA}	[34;42]	7.1 ± 0.9^{gA}	[6.3;7.9]	94.5 ± 1.6^{cA}	[92;96]
	Water storage	1.9 ± 0.4^{aA}	[1.5;2.2]	0.0 ± 0.0^{aA}	[0.0;0.2]	13.4 ± 3.4^{aA}	[9;17]	36.5 ± 6.0^{ghA}	[31;41]	35.3 ± 5.0^{hC}	[30;39]	96.8 ± 1.6*^{eB}	[94;98]
	Thermal cycling	3.0 ± 0.3^{aB}	[2.8;3.3]	0.1 ± 0.0^{aB}	[0.0;0.2]	13.0 ± 1.7^{aA}	[10;15]	37.1 ± 4.5^{fgA}	[32;41]	24.9 ± 2.7^{iB}	[21;27]	95.4 ± 1.0^{dA}	[93;97]
aPG	Initial	29.3 ± 4.8^{dB}	[25;33]	0.8 ± 0.1^{dB}	[0.6;1.0]	63.9 ± 8.6^{dA}	[56;71]	23.5 ± 2.2^{efA}	[20;26]	2.2 ± 0.5^{dA}	[1.7;2.7]	92.9 ± 2.4^{cB}	[90;95]
	Water storage	20.0 ± 3.4*^{eA}	[17;23]	0.5 ± 0.0*^{dA}	[0.4;0.6]	58.3 ± 8.1^{dA}	[51;65]	28.3;3.4^{efB}	[24;31]	8.9 ± 0.9^{eB}	[8.1;9.7]	93.9 ± 2.5*^{dB}	[91;96]
	Thermal cycling	19.3 ± 1.3^{cA}	[17;21]	0.7 ± 0.0*^{cB}	[0.6;0.9]	58.9 ± 5.5^{cA}	[53;63]	29.1 ± 3.9^{deB}	[25;33]	7.5 ± 1.6^{gB}	[6.2;8.8]	89.8 ± 2.0^{bA}	[87;92]
aPP	Initial	63.4 ± 3.5^{eC}	[60;66]	1.5 ± 0.1^{fC}	[1.4;1.7]	91.9 ± 5.8^{fC}	[86;97]	41.2 ± 1.7^{hA}	[38;43]	4.6 ± 2.0^{efA}	[3.0;6.2]	72.3 ± 3.1^{aA}	[68;75]
	Water storage	15.2 ± 1.9^{dA}	[13;17]	0.5 ± 0.0^{cA}	[0.3;0.6]	56.7 ± 6.8^{dA}	[50;62]	41.8 ± 0.8^{hA}	[40;43]	12.4 ± 1.4^{fB}	[10;14]	74.2 ± 1.8^{aA}	[71;76]
	Thermal cycling	36.6 ± 3.5^{dB}	[33;39]	1.2 ± 0.1^{dB}	[1.1;1.4]	78.0 ± 14.8^{deB}	[66;89]	44.6 ± 1.3^{hB}	[42;46]	3.1 ± 1.5^{eA}	[1.9;4.3]	75.6 ± 3.2^{aA}	[72;79]
aVS	Initial	90.7 ± 3.3^{hB}	[87;93]	2.4 ± 0.0^{hB}	[2.3;2.6]	126 ± 14.3^{gA}	[114;137]	30.3 ± 1.2^{gA}	[28;32]	4.7 ± 0.8^{fA}	[4.0;5.4]	81.0 ± 3.8^{bA}	[77;84]
	Water storage	80.9 ± 5.4^{hA}	[76;85]	2.2 ± 0.1*^{gA}	[2.0;2.4]	126 ± 3.3^{fA}	[122;129]	33.8 ± 1.0^{gB}	[32;35]	15.6 ± 1.6^{gB}	[13;17]	84.4 ± 3.3^{cB}	[80;87]
	Thermal cycling	80.6 ± 9.5^{fA}	[74;86]	2.2 ± 0.2^{fA}	[2.0;2.5]	131 ± 19.8*^{gA}	[115;146]	39.0 ± 1.8^{gC}	[36;41]	5.6 ± 3.5*^{fA}	[3.0;8.2]	92.5 ± 4.0^{cC}	[88;96]
aVC	Initial	12.4 ± 1.1^{cA}	[10;14]	0.4 ± 0.0^{cA}	[0.3;0.5]	42.0 ± 2.6^{bA}	[39;45]	23.1 ± 2.7^{efA}	[20;26]	3.4 ± 0.5^{eA}	[2.9;3.9]	80.2 ± 7.8^{bA}	[73;86]
	Water storage	13.1 ± 2.6*^{cB}	[10;15]	0.5 ± 0.1*^{cdB}	[0.3;0.6]	50.3 ± 2.5^{cB}	[47;53]	22.9 ± 1.7^{dA}	[20;25]	14.5 ± 1.0^{gB}	[12;16]	77.7 ± 5.3^{bA}	[72;82]
	Thermal cycling	20.3 ± 2.3^{cC}	[17;22]	0.7 ± 0.0^{cC}	[0.6;0.9]	71.5 ± 5.3^{dC}	[66;76]	32.1 ± 6.4^{efB}	[26;37]	17.1 ± 3.1^{hC}	[13;20]	94.0 ± 5.8^{bcdB}	[88;99]
bBC	Initial	83.9 ± 1.9^{gA}	[81;86]	2.5 ± 0.0^{iA}	[2.3;2.6]	122 ± 14.4^{gA}	[111;134]	10.6 ± 0.9^{cA}	[9.9;12]	0.1 ± 0.1^{abA}	[0;0.3]	-	-
	Water storage	86.5 ± 2.6^{iB}	[84;89]	2.5 ± 0.0*^{iB}	[2.4;2.7]	122 ± 9.5*^{fA}	[114;130]	12.9 ± 0.4^{cB}	[11;14]	1.5 ± 0.3^{cC}	[1.1;1.9]	-	-
	Thermal cycling	89.8 ± 2.2^{gC}	[87;92]	2.6 ± 0.0^{gC}	[2.5;2.8]	136 ± 8.3*^{gB}	[129;143]	14.1 ± 0.9^{cC}	[12;15]	0.5 ± 0.2^{dB}	[0.2;0.8]	-	-
bEP	Initial	66.0 ± 2.0^{fA}	[63;68]	1.4 ± 0.0^{eA}	[1.3;1.5]	80.5 ± 2.6^{eA}	[77;83]	6.6 ± 0.9^{bA}	[5.8;7.4]	0.0 ± 0.0^{aA}	[0;0.2]	-	-
	Water storage	67.5 ± 2.6^{gA}	[65;70]	1.5 ± 0.0^{eB}	[1.3;1.6]	84.5 ± 2.1*^{eC}	[81;87]	7.3 ± 0.1^{bB}	[7.1;7.5]	0.3 ± 0.1^{aB}	[0.1;0.5]	-	-
	Thermal cycling	66.4 ± 2.2^{eA}	[64;68]	1.4 ± 0.0^{eAB}	[1.3;1.6]	82.5 ± 4.5*^{eB}	[78;86]	7.6 ± 0.3*^{bC}	[7.2;7.9]	0.0 ± 0.1*^{abA}	[0;0.2]	-	-
bPC	Initial	106 ± 5.5^{kA}	[102;110]	2.7 ± 0.1^{jA}	[2.5;3.0]	171 ± 10.2^{iB}	[163;180]	23.5 ± 1.0^{efA}	[21;25]	0.5 ± 0.4^{cB}	[0.1;0.9]	-	-
	Water storage	106 ± 5.1*^{jA}	[102;110]	2.9 ± 0.1*^{kA}	[2.7;3.0]	159 ± 17.1*^{hA}	[145;172]	26.0 ± 1.3^{deB}	[24;27]	0.6 ± 0.3^{bB}	[0.3;1.0]	-	-
	Thermal cycling	108 ± 12.0^{hA}	[100;116]	3.0 ± 0.1^{jB}	[2.8;3.1]	179 ± 14.0^{iC}	[168;190]	26.5 ± 0.5^{dB}	[25;27]	0.1 ± 0.1^{bcA}	[0;0.3]	-	-
bTP	Initial	107 ± 4.2^{kA}	[103;110]	2.3 ± 0.1^{gB}	[2.1;2.4]	121 ± 3.7^{gA}	[117;125]	4.5 ± 0.2^{aA}	[4.3;4.8]	0.2 ± 0.1^{bcA}	[0;0.4]	-	-
	Water storage	108 ± 3.8^{jAB}	[104;111]	1.6 ± 0.0^{fA}	[1.4;1.7]	120 ± 9.5*^{fA}	[112;128]	4.8 ± 0.4^{aA}	[4.3;5.2]	0.4 ± 0.2^{abB}	[0.1;0.6]	-	-
	Thermal cycling	110 ± 2.4^{hB}	[107;112]	2.3 ± 0.0*^{fB}	[2.2;2.5]	124 ± 3.4^{fA}	[120;128]	4.5 ± 0.2^{aA}	[4.3;4.8]	0.1 ± 0.1^{bcA}	[0;0.3]	-	-
bTH	Initial	3.8 ± 1.1^{bA}	[3.0;4.5]	0.1 ± 0.0^{bA}	[0.0;0.3]	50.2 ± 3.2^{cB}	[46;53]	17.1 ± 1.0^{dA}	[15;18]	0.3 ± 0.2^{bcA}	[0.0;0.5]	-	-
	Water storage	6.6 ± 1.1^{bB}	[5.8;7.3]	0.3 ± 0.0^{bB}	[0.1;0.4]	38.5 ± 2.1^{bA}	[35;41]	30.3 ± 2.3^{fB}	[27;33]	3.1 ± 0.6 ^{dB}	[2.5;3.7]	-	-
	Thermal cycling	6.7 ± 1.5*^{bB}	[5.8;7.6]	0.3 ± 0.0*^{bB}	[0.1;0.4]	48.0 ± 4.3^{bB}	[43;52]	28.6 ± 9.5^{deB}	[20;36]	0.2 ± 0.2*^{abcA}	[0.0;0.5]	-	-
cPP	Initial	99.7 ± 3.3*^{iC}	[96;102]	2.8 ± 0.1*^{jB}	[2.6;3.0]	151 ± 11.3*^{hA}	[141;160]	23.3 ± 0.3^{fA}	[22;24]	0.1 ± 0.1*^{aA}	[0.0;0.2]	-	-
	Water storage	63.6 ± 4.6^{fA}	[59;67]	2.6 ± 0.1^{jA}	[2.4;2.8]	159 ± 8.6^{ghA}	[152;166]	26.7 ± 0.5^{eB}	[25;28]	0.3 ± 0.2^{aB}	[0.0;0.6]	-	-
	Thermal cycling	85.9 ± 14.6*^{fgB}	[76;95]	2.9 ± 0.0^{iC}	[2.8;3.0]	153 ± 11.6^{hA}	[143;162]	26.2 ± 0.5^{dB}	[24;27]	0.0 ± 0.0*^{aA}	[0.0;0.2]	-	-
cPB	Initial	102 ± 2.4^{jC}	[100;105]	2.8 ± 0.1^{jC}	[2.7;3.0]	143 ± 12.8^{hA}	[132;153]	22.5 ± 1.5*^{eA}	[20;24]	0.3 ± 0.2^{cA}	[0.1;0.5]	-	-
	Water storage	83.1 ± 7.3^{hiA}	[77;88]	2.3 ± 0.1^{hA}	[2.2;2.5]	153 ± 7.5^{gA}	[146;159]	26.3 ± 0.8^{eB}	[24;27]	0.4 ± 0.2^{abA}	[0.1;0.7]	-	-
	Thermal cycling	91.9 ± 11.1*^{gB}	[84;99]	2.8 ± 0.0^{hB}	[2.6;2.9]	149 ± 10.5^{hA}	[140;157]	25.9 ± 0.7^{dB}	[24;27]	0.3 ± 0.2^{cA}	[0.0;0.5]	-	-

*Deviation from the normal distribution.
[abcdefghijk]Different small letters indicate significant differences between the materials within one aging regime.
[ABC] Different capital letters indicate significant differences between the aging regimes within one material.
CI Confidence interval.
SD Standard deviation.

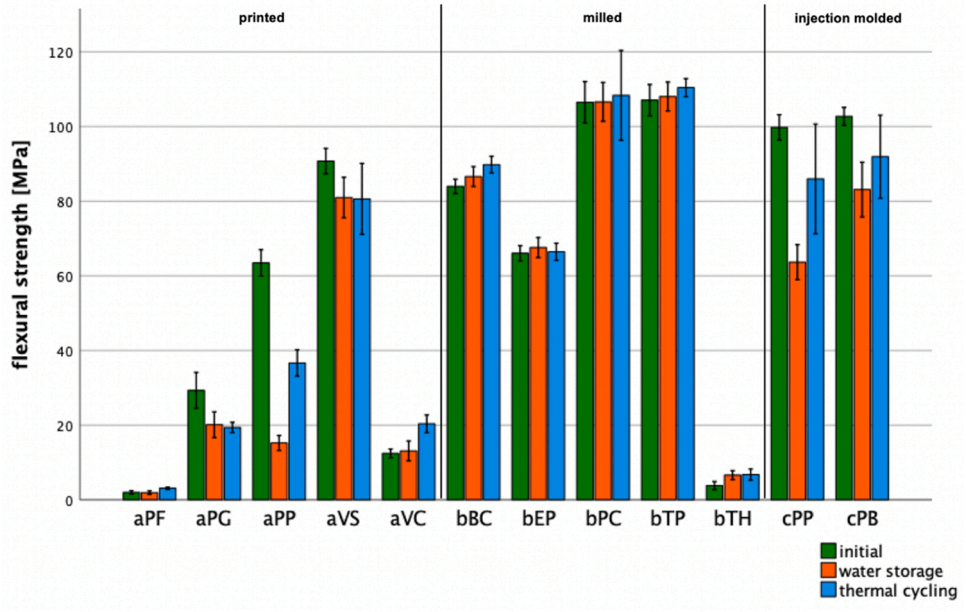

Fig. 5. Mean FS values and standard deviations of tested materials for occlusal devices at baseline and after aging.

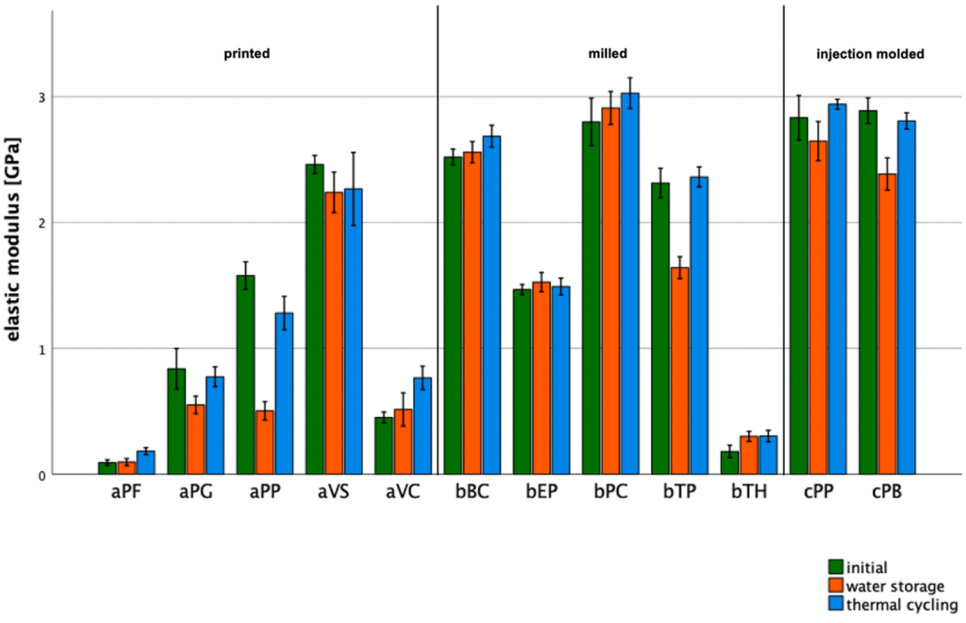

Fig. 6. Mean E values and standard deviations of tested materials for occlusal devices at baseline and after aging.

the other materials followed by bTH and aVC ($p < 0.001$–0.008). aPP and aPG showed lower HM values compared to bEP, bTP, aVS, bBC, cPB, cPP and bPC ($p < 0.001$). bTP, aVS, bBC, cPB, cPP and bPC presented higher HM values than bEP ($p < 0.001$). The injection molded materials and bPC showed higher values compared to bTP, aVS and bBC ($p < 0.001$). Only bPC presented higher HM values compared to the injection molded materials ($p = 0.041$).

Within the thermal cycling group also aPF showed the lowest values compared to the other materials followed by bTH and aPG ($p < 0.001$). aVC revealed lower HM values than bEP, bTP, aVS, bBC, cPB, cPP and bPC ($p < 0.001$). bTP, aVS, bBC, cPB, cPP and bPC showed higher values compared to aPP and bEP ($p < 0.001$). aVS, bBC, cPB, cPP and bPC presented higher values than bTP ($p < 0.001$–0.023). Higher HM values were observed for the injection molded materials and bPC than for aVS and bBC ($p < 0.001$–0.010). Only bPC presented higher values than the injection molded materials ($p < 0.001$).

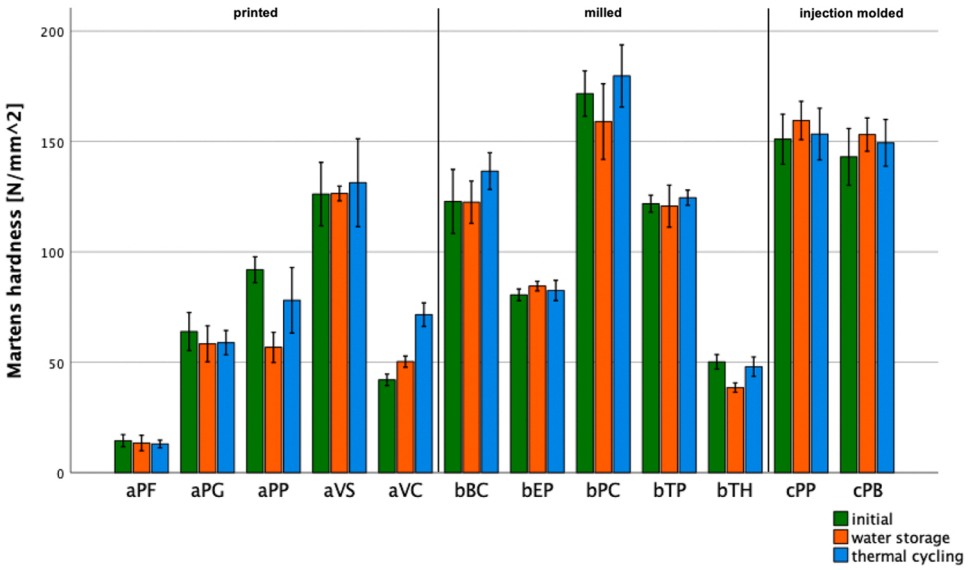

Fig. 7. Mean HM values and standard deviations of tested materials for occlusal devices at baseline and after aging.

3.3.2. *Impact of artificial aging on Martens hardness*

Artificial aging significantly affected the Martens hardness values of the materials except for aPG, aPF, aVS, bTP, cPP and cPB ($p = 0.053–0.471$) (Table 3, Fig. 7). The highest Martens hardness values for aPP were observed in the initial group and the lowest values were calculated after water storage ($p < 0.001–0.011$). The highest Martens hardness values were observed after thermal cycling and the lowest values were calculated in the initial group for aVC ($p < 0.001$). After thermal cycling, the Martens hardness values were the highest compared to water storage and initial aging for bBC ($p = 0.003–0.011$). The highest Martens hardness values were observed after thermal cycling and the lowest values were calculated in the water storage group for bPC ($p = 0.001–0.049$). bTH presented the highest Martens hardness values in the thermal cycling and initial group compared to water storage ($p < 0.001$). bEP showed the highest Martens hardness values after water storage and the lowest in the initial group ($p = 0.004–0.036$).

3.4. *Comparison of water sorption of all tested materials*

3.4.1. *Impact of the material on water sorption*

Within the initial group bTP showed the lowest w_{sp} values compared to the other materials followed by bEP, bBC and bTH ($p < 0.001$) (Table 3, Fig. 8). cPB presented lower values compared to cPP, aVS, aPF and aPP ($p < 0.001–0.023$). aVC, aPG, bPC and cPP showed lower values than aVS, aPF and aPP ($p < 0.001$). Only aPF and aPP revealed higher w_{sp} values than aVS within the initial group ($p < 0.001$).

After water storage, bTP showed the lowest w_{sp} values compared to the other materials followed by bEP and bBC ($p < 0.001$). aVC revealed lower values than cPB, cPP, aPG, bTH, aVS, aPF and aPP ($p < 0.001$). bTH, aVS, aPF and aPP showed higher values compared to bPC, cPB and cPP ($p < 0.001$). aVS, aPF and aPP presented higher values than aPG and bTH ($p < 0.001–0.002$). Only aPP showed higher values compared to aVS ($p < 0.001$).

Within the thermal cycling group bTP showed the lowest w_{sp} values compared to the other materials followed by bEP and bBC ($p < 0.001$). aVC, aPF, aVS and aPP presented higher values than cPB, cPP, and bPC

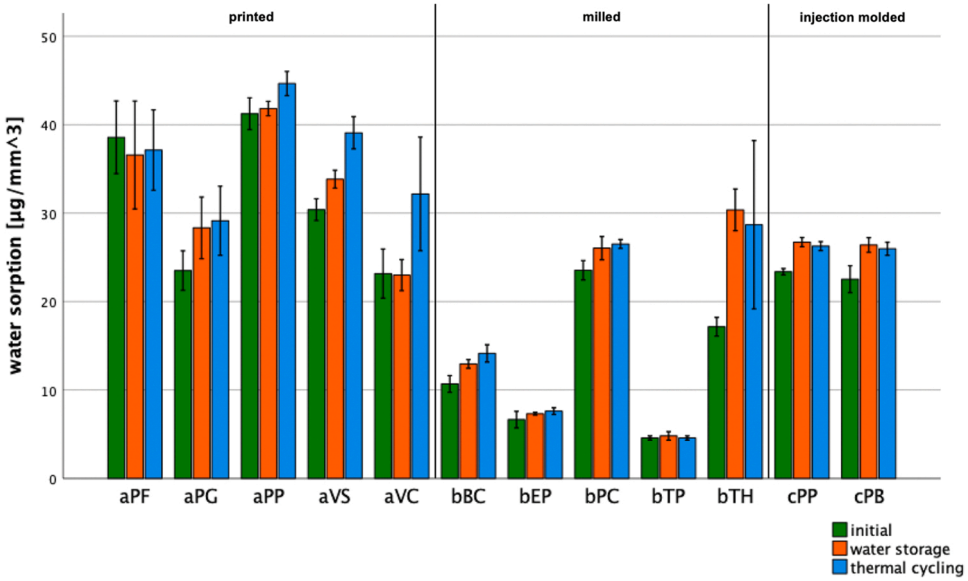

Fig. 8. Mean w_{sp} values and standard deviations of tested materials for occlusal devices at baseline and after aging.

($p < 0.001$–0.023). Higher w_{sp} values were observed for aPF, aVS and aPP than for aPG and bTH ($p < 0.001$–0.049). aVC showed lower values than aVS and aPP ($p < 0.001$–0.019). Only aPP showed higher values compared to aPF and aVS ($p < 0.001$).

3.4.2. Impact of artificial aging on water sorption

Artificial aging significantly affected the w_{sp} values of the materials except for aPF and bTP ($p = 0.394$–0.671) (Table 3, Fig. 8). The lowest w_{sp} values were observed in the initial group and the highest values were calculated after water storage and thermal cycling for aPG, bPC, bTH, cPP and cPB ($p < 0.001$–0.003). aPP and aVC showed the lowest values in the initial and water storage group and the highest w_{sp} values after thermal cycling ($p < 0.001$–0.004). The lowest w_{sp} values were calculated in the initial group and the highest values were presented after thermal cycling for aVS, bBC and bEP ($p < 0.001$–0.034).

3.5. Comparison of water solubility of all tested materials

3.5.1. Impact of the material on water solubility

Within the initial group bEP and cPP showed lower values compared to bTP, bTH, cPB, bPC, aPG, aVC, aPP, aVS and aPF ($p < 0.001$–0.026) (Table 3, Fig. 9). bBC presented lower values than cPB, bPC, aPG, aVC, aPP, aVS and aPF ($p < 0.001$–0.027). bTP, bTH, cPB and bPC showed lower values than aPG, aVC, aPP, aVS and aPF ($p < 0.001$). aPG revealed lower values compared to aVC, aPP, aVS and aPF ($p < 0.001$). aVS and aPF showed higher values than aVC ($p < 0.001$–$0,002$), while only aPF presented higher values compared to aPP and aVS ($p < 0.001$–0.004).

After water storage, lower w_{sl} values were observed for cPP and bEP than for bPC, bBC, bTH, aPG, aPP, aVC, aVS and aPF ($p < 0.001$–0.023). bTP, cPB and bPC showed lower values compared to bBC, bTH, aPG, aPP, aVC, aVS and aPF ($p < 0.001$). bBC presented lower values than bTH, aPG, aPP, aVC, aVS and aPF ($p < 0.001$), followed by bTH, aPG and aPP ($p < 0.001$–0.003). Only aPF had higher values than aVC and aVS ($p < 0.001$).

After thermal cycling, lower values were obtained for cPP than for bPC, bTP, cPB, bBC, aPP, aVS, aPG, aVC and aPF ($p < 0.001$–0.026). bEP showed lower values than cPB, bBC, aPP, aVS, aPG, aVC, aPF ($p < 0.001$–0.019). bTH, bPC, bTP and cPB presented lower values compared to bBC, aPP, aVS, aPG, aVC and aPF ($p < 0.001$–0.034). bBC revealed lower values compared to aPP, aVS, aPG, aVC and aPF ($p < 0.001$), followed by aPP, aVS, aPG, aVC and aPF ($p < 0.001$–0.041).

3.5.2. Impact of artificial aging on water solubility

Artificial aging significantly affected the w_{sl} values of the materials except for cPB ($p = 0.429$) (Table 3, Fig. 9). The lowest w_{sl} values were observed in the initial group and the highest values were calculated after water storage and thermal cycling for aPG ($p < 0.001$). aPF, aPP and bBC showed the lowest values in the initial group and the highest after water storage ($p < 0.001$–0.049). The lowest w_{sl} values were calculated in the initial and thermal cycling group and the highest values were shown after water storage for aVS, bTP, bEP, bTH and cPP ($p < 0.001$–0.016). aVC showed the lowest values in the initial group and the highest after thermal cycling ($p < 0.001$–0.010). bPC presented the lowest values after thermal cycling compared to the other aging regimes ($p = 0.001$–0.048).

3.6. Comparison of conversion rate of printed materials

3.6.1. Impact of the material on the conversion rate

After all aging regimes, aPP showed the lowest DC values compared to the remaining printed materials ($p < 0.001$–0.023) (Table 3, Fig. 10). Within the initial group aVC and aVS presented lower values than aPG and aPF ($p < 0.001$). After water storage, aVC showed lower values compared to aVS, aPG and aPF ($p < 0.001$–0.002), followed by aVS, aPG and aPF ($p < 0.001$–0.019). Within the thermal cycling group aPG revealed lower values than aVS and aPF ($p < 0.001$–0.028). Only aPF showed higher values compared to aVS ($p = 0.005$).

3.6.2. Impact of artificial aging on the conversion rate

Artificial aging significantly affected the DC values of the materials except for aPP ($p = 0.217$) (Table 3, Fig. 10). After water storage, aPF showed the highest DC values compared to the other aging regimes ($p = 0.010$–0.019). The highest DC values were observed in the initial group and after water storage for aPG ($p = 0.002$–0.007). aVS presented the highest DC values after thermal aging and the lowest in the initial group ($p < 0.001$–0.049). After thermal cycling, aVC showed the highest values compared to the remaining aging regimes ($p < 0.001$–0.001).

3.7. Spearman's correlation between all tested parameters within pooled materials

Positive correlations between FS and HM ($p < 0.001$, $R = 0.854$), FS

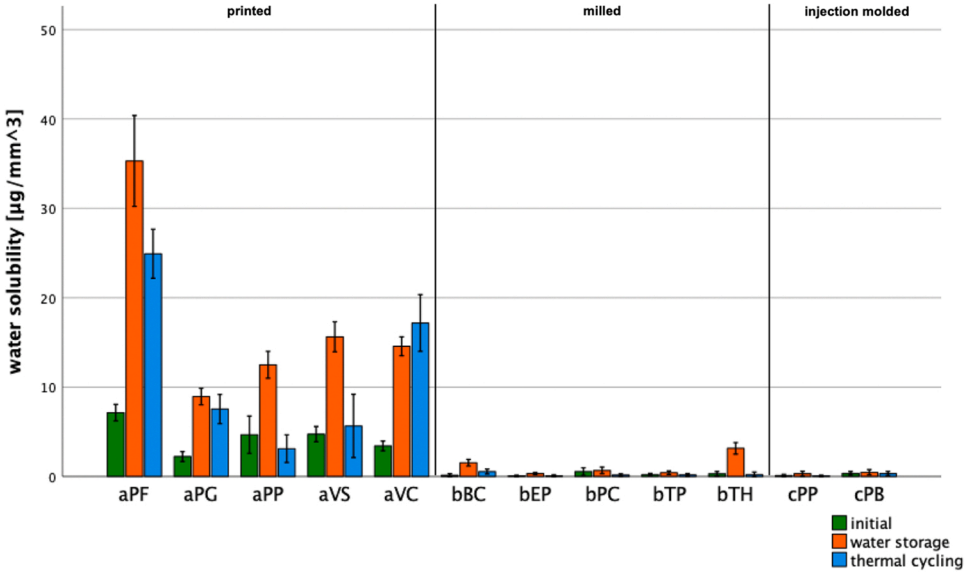

Fig. 9. Mean w_{sl} values and standard deviations of tested materials for occlusal devices at baseline and after aging.

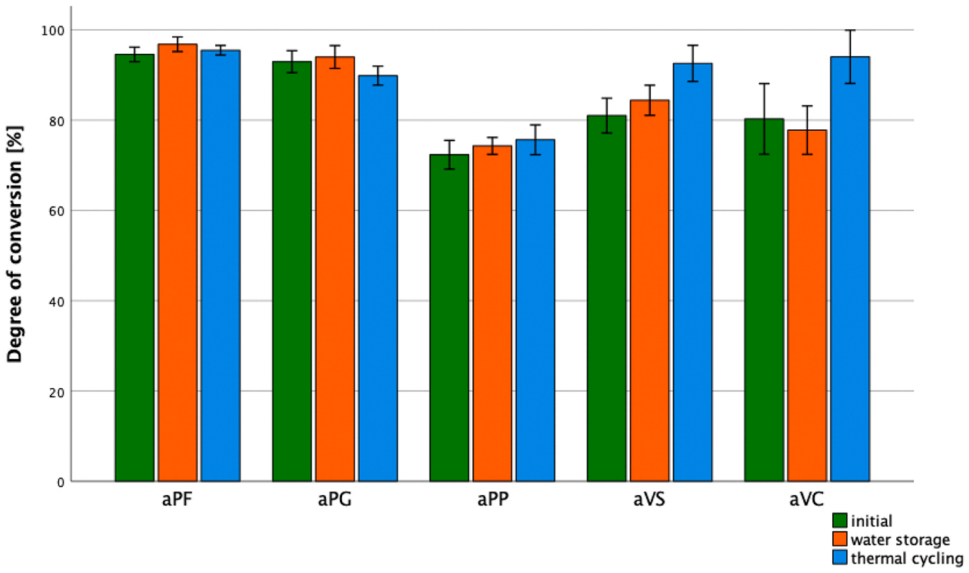

Fig. 10. Mean DC values and standard deviations of printed materials for occlusal devices at baseline and after aging.

and E ($p < 0.001$, $R = 0.820$) as well as w_{sp} and w_{sl} ($p < 0.001$, $R = 0.627$) were observed. Negative correlations between FS and w_{sp} ($p < 0.001$, $R = -0.446$), FS and w_{sl} ($p < 0.001$, $R = -0.532$), E and w_{sp} ($p < 0.001$, $R = -0.207$), E and w_{sl} ($p < 0.001$, $R = -0.493$), HM and w_{sp} ($p < 0.001$, $R = -0.218$) as well as HM and w_{sl} ($p < 0.001$, $R = -0.503$) were found.

4. Discussion

The aim of this investigation was to examine the physical properties of five 3D-printed, five milled and two injection molded splint materials for oral appliances. The tested null hypotheses stating that neither the choice of material nor artificial aging procedure showed a significant impact on FS, E, HM, w_{sp}, w_{sl} and DC were rejected.

No ISO standard has been established for splint materials till today. Therefore, the ISO standard for denture base polymers was used to evaluate FS and E [3,5,10]. According to ISO 20795-1:2013 the values of hot polymerizable, thermoplastic moldings or granulates, light and microwave polymerizable polymers must be at least 65 MPa for FS and 2 GPa for E. The values of auto-polymerizable polymers must be at least 60 MPa for FS and 1.5 GPa for E. aPF, aPG, aPP, aVC and bTH showed FS and E values below 65 MPa and 2 GPa initially and after all aging regimes. Considering E, bEP also didn't surpass the 2 GPa mark after all aging regimes and bTP showed E values below 2 GPa after water storage. As these materials did not fracture during the test, FS was calculated by the force at maximum deflection. The geometry of the specimen holder allowed a maximum deflection of 10 mm. The load-deflection curves represent the different behaviors of the materials (Fig. 11). These low calculated FS values could not be disadvantageous as no fracture occurred. However, this depends on whether there is a

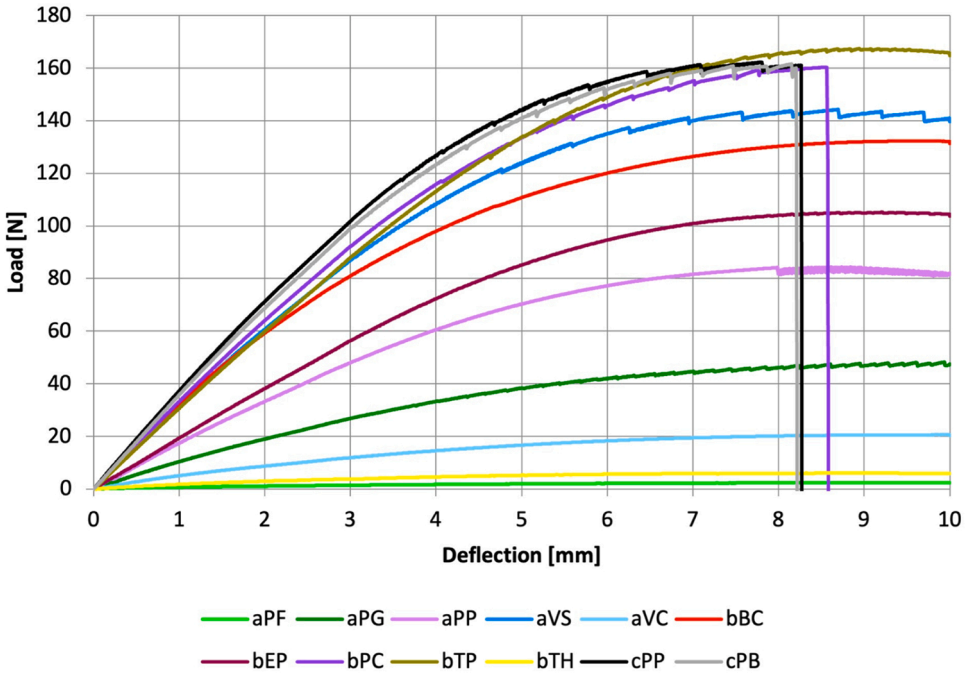

Fig. 11. Load-deflection curves of the initial group for each material.

permanent deformation or whether the material returns to its original position [18]. During the measurement, specimens made of aVS (3 specimens in the initial group, 11 water stored and 8 thermal cycled specimens), bPC (9 specimens in the initial group, 13 water stored and 15 thermal cycled specimens), cPP (13 specimens in the initial group, 15 water stored and 15 thermal cycled specimens) and cPB (13 specimens in the initial group, 15 water stored and 14 thermal cycled specimens) fractured. This suggests that PMMA-based materials (bPC, cPP, cPB) do not show high ductility. This is supported by the fact, that these materials showed the highest E values. aVS was the only printed material which surpassed the limit of 65 MPa and 2 GPa. Interestingly, the number of fractured aVS specimens increased significantly after aging while the FS and E values decreased. W_{sl} increased after water storage and w_{sp} and DC increased after all aging regimes for aVS. This might have led to an increasing brittleness of the material and thus to an increasing number of fractured specimens. The high FS and E compared to the other printed materials can be explained by the composition of aVS, as cross-linked polymer chains and inorganic fillers can increase the strength of the resin [19]. To make a better conclusion, more precise information from the manufacturer on the composition would be useful. This differs from a previous study where aVS only achieved a FS of 37 MPa [13]. However, an explanation could be the different printing direction of the specimens. The literature shows a relevant influence of the printing direction on FS values and that the highest are achieved with a vertical orientation on the building platform [20,21]. This could have caused the higher values in the present study. bTP and bPC showed the highest FS values after all aging regimes, with the difference that the bTP specimens did not fracture. This speaks for the ductility and thus a lower risk of fracture, better resistance to crack propagation and simultaneously high strength of PC based materials [10]. This is supported by the result that bTP showed lower E values than bPC. bEP and bBC showed no fracture, which might prove the ductility of POM-C and PET-G based materials. The injection molded PMMA-based materials showed lower FS values compared to the milled PMMA-based bPC after all aging regimes and lower E values after water storage and thermal cycling, which is consistent with previous investigations [10,13]. This can be explained by the industrial production under high temperatures and pressure, resulting in a dense polymer network of the milled specimens [10,15]. While this finding acknowledges the potential advantages of CAD/CAM milled devices, previous investigations showed no significant difference between the FS values of injection molded and milled PMMA-based materials [3,5]. The present study also showed no significant difference between the E values of bPC, cPP and cPB in the initial group. This calls for further investigations.

bPC showed the highest Martens values after all aging regimes followed by the injection molded materials. This result agrees with a previous investigation, in which the milled PMMA material presented higher Vickers hardness compared to the injection molded PMMA material [13]. This is attributed to the industrial production of PMMA blocks under high pressure, which results in fewer proceflaws and reduced voids in the material [5,13].

The lower HM values observed for bTP compared to the milled and injection molded PMMA materials are consistent with a previous publication in which PC-based milled materials showed a lower surface hardness than injection molded PMMA material [10]. The conclusion of another research study in which lower elastic modulus values were obtained for injection molded PC-based denture base resins compared to conventional PMMA material, underlines the assumption that the composition of the material has a significant influence on its hardness and is more relevant than the manufacturing method [22]. As a previous publication reported higher Martens hardness values for bTP compared to the injection molded PMMA material, further investigations are necessary to investigate the cause for these findings more closely [5]. bBC showed similar Martens hardness values as bTP. Milled PC and POM-C-based materials thus have similar hardness behavior, with HM values of bBC even being superior to bTP after thermal cycling. aVS was the only printed material with similar HM values to bTP and bBC, thus refuting the statement of earlier publications that 3D-printed resins generally have lower mechanical properties compared to other materials [5,11,13]. The high HM values of aVS can be explained by the composition of the resin as for example with a higher filler content [15,17]. However, due to the insufficient manufacturer's data, this cannot be definitively determined.

Except for bTH, the PET-G based bEP showed the lowest hardness values in the group of milled materials and similar values to the printed aPP. The 3D-printed materials aPF, aVC, aPG and the milled bTH showed the lowest HM values with aPF being by far the softest material. However, the higher HM values of aPP compared to aPF, aVC and aPG contrast with the positive correlation between DC and hardness shown in the literature. In the present investigation, aPP showed the lowest DC values after all aging regimes. Further studies on the correlation between DC and HM are therefore required. Low HM values speak for the elastic-plastic behavior of the materials [15]. With high forces occurring during bruxism, the antagonistic teeth could thus be protected from abrasion by a soft splint material. The manufacturers also advertise an increased wearing comfort of the splints due to the plastic behavior. However, this low HM could correlate with the increased wear of the soft splint materials shown in the literature during 2-body wear [4,7,12], as hardness is related to its resistance to abrasion by the antagonist jaw [23]. Further studies are required to find out if there is a positive correlation between hardness and abrasion of occlusal device materials. This is highly clinically relevant, as volumetric and vertical loss can cause a shift in the statics and dynamics of the splint, as well as a release of monomer particles from the splint material [12]. Investigations have shown that in 3D-printing, the layer thickness, the printing angle and the post-curing method have an influence on hardness. A 50 µm layer thickness, a 45° printing angle and a post-polymerisation in an inert atmosphere resulted in higher hardness values [11,14]. Therefore, precise information on these parameters should be provided by the manufacturer.

Generally, the exposure of a material to a humid environment leads to a degradation of the mechanical properties. For the materials aPF, aVC, bBC, bTP and bTH, an increase in the FS values after thermal cycling and for aVC, bBC and bTH after water storage was observed. The E values of aPF, aVC, bBC, bPC, bTH and cPP also increased after thermal cycling and of aVC, bBC, bEP and bTH after water storage compared to the initial group. The HM values of aVC, bBC, bPC and bEP after thermal cycling and of aVC and bEP after water storage also increased. Previous studies describe a correlation between higher temperature and increasing flexibility and softening of the material [24]. The increased FS and E values and thus the increased stiffness after thermocycling could therefore be explained by the alternately immersion of the specimen basket in the cold 5 °C water bath. Further investigations are necessary to investigate the cause for these findings. The increased mechanical values for aVC could be explained by the increased DC values after aging. The decrease in w_{sl} for bPC after thermal cycling compared to the initial group could be the explanation for the higher HM and E values after thermal cycling. Aging showed no significant influence on the FS values of bPC and bEP and no significant influence on the HM values of aPF, aPG, aVS bTP, cPP and cPB, which speaks for the long-term stability of the materials in the moist environment of the oral cavity. The remaining materials showed a decrease in mechanical properties after aging. The 3D-printed materials, except aVC and aPF, and injection molded group, were more susceptible to aging regarding FS compared to the milled group. In general, it can be concluded that aging did not lead to a large decrease in hardness for all materials, except for aPP.

Regardless the aging regime, bTP, followed by bEP and bBC, showed the lowest w_{sp} values compared to the other remaining materials. This leads to the assumption that PC, PET-G and POM tend to absorb less water in clinical situations and thus show a better long-term stability in the oral environment. Low water sorption and solubility can be

attributed to the high degree of polymerization of these materials [25]. High DC values mean a higher conversion of monomers to polymers and thus better mechanical properties and biocompatibility [26]. In comparison, higher w_{sp} values of bPC and bTH were calculated in this investigation. Especially bPC showed similar w_{sp} values compared to the injection molded PMMA materials. Similar results for PC-based materials as well as comparatively higher w_{sp} values for PMMAs were already obtained in previous investigations [5,10]. 3D-printed resins showed different behaviors. aVS, aPF and aPP presented the highest w_{sp} values after all aging regimes, supporting prior results that 3D-printed resins absorb a greater amount of water [18,20]. Microscopic voids between the resin layers as well as lower DC values could be the explanation for the higher w_{sp} values compared to milled and injection molded materials [20]. For aPG and aVC the sorption values were similar to that of bPC, bTH and the injection molded materials. This is an interesting result as aVC and aVS as well as aPG and aPF showed no significant difference in the initial DC values. aPF even showed the highest DC rates after all aging regimes. Only aPP showed inferior DC values after all aging regimes. A previous study, which analyzed the effect of monomer type on DC, w_{sp} and w_{sl}, concluded that not only the conversion but also the chemical composition, the hydrophilic characteristics of the monomers and the polymer network influence the composites sorption and solubility behavior. [27]. The different composition of the 3D-printed resins can therefore be used as an explanation for the varying w_{sp} values. Further research is necessary to investigate the cause for these findings more closely. In contrast, all 3D-printed materials showed higher w_{sl} values than pressed and injection molded materials, with aPF showing by far the highest solubility regardless of the aging regime. The lowest w_{sl} values after all aging regimes were obtained for bEP and cPP, but it must also be mentioned that there were no major differences between the milled and injection molded materials. A negative correlation between w_{sp} and w_{sl} of the materials aPP and aVS is observed, with w_{sp} being higher in the water storage group compared to the thermocycling group, whereas w_{sl} was higher in the thermocycling group than in the water storage group. The correlation between w_{sp} and w_{sl} requires further investigations. By using a reduced layer thickness, lower w_{sp} and w_{sl} values could be achieved for printed materials. This is explained by the fact that the light intensity during the printing process decreases with increasing layer thickness, as it is absorbed and scattered by a larger amount of resin particles, which leads to a gradation of the curing from the surface towards the inside [14]. As there are plenty of elastic-plastic splint materials on the dental market, international standards for occlusal devices should be established.

Since the clinical indication of splints is not only bruxism, but also the correction of tooth and jaw misalignments (e.g., aligner therapy) or the testing of a new bite position before the insertion of a definitive restoration, patients wear them for up to 23 h. Therefore, the aging of the materials by thermal cycling is relevant. Here, 5000 cycles correspond to 6 months in vitro [18,28,29]. The decision for a material should be made regarding the clinical situation. All 3D-printed materials, except for aVS, and the milled bTH showed low mechanical properties. Due to the low E and HM values in particular, the clinical use of these materials for patients with severe bruxism should be considered critically as the materials have to withstand high masticatory forces of up to 770 N. The use of these soft splint materials for patients with craniomandibular dysfunction should be investigated as part of in vivo studies. The clinical indication of the splint should therefore be the deciding criteria for the choice of material.

However, a limitation of the study is the consistent exposure to moisture, especially during the 90-day storage period, as splints are not worn continuously for 3 months. Further research is necessary to investigate whether the properties of the 3D-printed materials are influenced by wet-grounding, as it is unknown how deep printed specimens are polymerized during post-processing. In this investigation the Spearman's correlation between all tested parameters was performed within pooled materials. Further research investigating the correlations of the properties within each material are recommended. The DC of the milled and injection molded materials could not be determined, as the Raman spectra of the monomer of cPP and cPB showed no detectable peaks and as the unpolymerized resin of the milled blank wasn't available.

5. Conclusion

Within the limitations in this in vitro study, the following conclusions were drawn:

1. The composition of the materials influences the mechanical and physical properties, as large differences were found among the 3D-printed and milled groups.
2. The printed aVS showed similar mechanical properties as the milled materials.
3. 3D-printed materials showed higher w_{sp} and w_{sl} values compared to the milled and injection molded group.
4. The 3D-printed materials, except aVC and aPF, and the injection molded groups, were more susceptible to aging regarding FS compared to the milled group.
5. Aging did not lead to a large decrease in hardness, except for aPP.

Ethical approval

This article does not contain any studies with human participants or animals performed by any of the authors.

Acknowledgements

The authors thank bredent, Dental Plus, Ivoclar Vivadent, pro3dure, VOCO and Zirkonzahn for supporting this investigation. This research did not receive any specific grant from funding agencies in the public, commercial, or not-for-profit sectors.

Informed consent

For this type of study, formal consent was not required.

References

[1] Singh PK, Alvi HA, Singh BP, Singh RD, Kant S, Jurel S, et al. Evaluation of various treatment modalities in sleep bruxism. J Prosthet Dent 2015;114:426–31.
[2] Carra MC, Bruni O, Huynh N. Topical review: sleep bruxism, headaches, and sleep-disordered breathing in children and adolescents. J Orofac Pain 2012;26:267–76.
[3] Prpic V, Slacanin I, Schauperl Z, Catic A, Dulcic N, Cimic S. A study of the flexural strength and surface hardness of different materials and technologies for occlusal device fabrication. J Prosthet Dent 2019;121:955–9.
[4] Huettig F, Kustermann A, Kuscu E, Geis-Gerstorfer J, Spintzyk S. Polishability and wear resistance of splint material for oral appliances produced with conventional, subtractive, and additive manufacturing. J Mech Behav Biomed Mater 2017;75:175–9.
[5] Berli C, Thieringer FM, Sharma N, Müller JA, Dedem P, Fischer J, et al. Comparing the mechanical properties of pressed, milled, and 3D-printed resins for occlusal devices. J Prosthet Dent 2020;124:780–6.
[6] Rosentritt M, Behr M, Strasser T, Schmid A. Pilot in-vitro study on insertion/removal performance of hand-cast, milled and 3D printed splints. J Mech Behav Biomed Mater 2021;121:104612.
[7] Lutz AM, Hampe R, Roos M, Lümkemann N, Eichberger M, Stawarczyk B. Fracture resistance and 2-body wear of 3-dimensional-printed occlusal devices. J Prosthet Dent 2019;121:166–72.
[8] Strub JR, Rekow ED, Witkowski S. Computer-aided design and fabrication of dental restorations: current systems and future possibilities. J Am Dent Assoc 2006;137:1289–96.
[9] Kessler A, Hickel R, Reymus M. 3D printing in dentistry-state of the art. Oper Dent 2020;45:30–40.
[10] Gibreel M, Perea-Lowery L, Vallittu PK, Lassila L. Characterization of occlusal splint materials: CAD-CAM versus conventional resins. J Mech Behav Biomed Mater 2021;124:104813.
[11] Grymak A, Aarts JM, Ma S, Waddell JN, Choi JJE. Comparison of hardness and polishability of various occlusal splint materials. J Mech Behav Biomed Mater 2021;115:104270.

[12] Grymak A, Waddell JN, Aarts JM, Ma S, Choi JJE. Evaluation of wear behaviour of various occlusal splint materials and manufacturing processes. J Mech Behav Biomed Mater 2022;126:105053.
[13] Wesemann C, Spies BC, Sterzenbach G, Beuer F, Kohal R, Wemken G, et al. Polymers for conventional, subtractive, and additive manufacturing of occlusal devices differ in hardness and flexural properties but not in wear resistance. Dent Mater 2021;37:432–42.
[14] Perea-Lowery L, Gibreel M, Vallittu PK, Lassila L. Evaluation of the mechanical properties and degree of conversion of 3D printed splint material. J Mech Behav Biomed Mater 2021;115:104254.
[15] Reymus M, Stawarczyk B. In vitro study on the influence of postpolymerization and aging on the Martens parameters of 3D-printed occlusal devices. J Prosthet Dent 2021;125:817–23.
[16] Hampe R, Lümkemann N, Sener B, Stawarczyk B. The effect of artificial aging on Martens hardness and indentation modulus of different dental CAD/CAM restorative materials. J Mech Behav Biomed Mater 2018;86:191–8.
[17] Reymus M, Stawarczyk B. Influence of different postpolymerization strategies and artificial aging on hardness of 3D-printed resin materials: an in vitro study. Int J Prosthodont 2020;33:634–40.
[18] Greil V, Mayinger F, Reymus M, Stawarczyk B. Water sorption, water solubility, degree of conversion, elastic indentation modulus, edge chipping resistance and flexural strength of 3D-printed denture base resins. J Mech Behav Biomed Mater 2023;137:105565.
[19] Alp G, Murat S, Yilmaz B. Comparison of flexural strength of different CAD/CAM PMMA-based polymers. J Prosthodont 2019;28:e491–5.
[20] Väyrynen VO, Tanner J, Vallittu PK. The anisotropicity of the flexural properties of an occlusal device material processed by stereolithography. J Prosthet Dent 2016;116:811–7.
[21] Unkovskiy A, Bui PH, Schille C, Geis-Gerstorfer J, Huettig F, Spintzyk S. Objects build orientation, positioning, and curing influence dimensional accuracy and flexural properties of stereolithographically printed resin. Dent Mater 2018;34:e324–33.
[22] Hamanaka I, Takahashi Y, Shimizu H. Mechanical properties of injection-molded thermoplastic denture base resins. Acta Odontol Scand 2011;69:75–9.
[23] Zinelis S, Panayi N, Polychronis G, Papageorgiou SN, Eliades T. Comparative analysis of mechanical properties of orthodontic aligners produced by different contemporary 3D printers. Orthod Craniofac Res 2022;25:336–41.
[24] Perea-Lowery L, Gibreel M, Garoushi S, Vallittu P, Lassila L. Evaluation of flexible three-dimensionally printed occlusal splint materials: an in vitro study. Dent Mater 2023;39:957–63.
[25] Hada T, Kanazawa M, Iwaki M, Katheng A, Minakuchi S. Comparison of mechanical properties of PMMA disks for digitally designed dentures. Polymers 2021;13.
[26] Aati S, Akram Z, Shrestha B, Patel J, Shih B, Shearston K, et al. Effect of post-curing light exposure time on the physico-mechanical properties and cytotoxicity of 3D-printed denture base material. Dent Mater 2022;38:57–67.
[27] Fonseca AS, Labruna Moreira AD, de Albuquerque PP, de Menezes LR, Pfeifer CS, Schneider LF. Effect of monomer type on the CC degree of conversion, water sorption and solubility, and color stability of model dental composites. Dent Mater 2017;33:394–401.
[28] Gad MM, Fouda SM, Abualsaud R, Alshahrani FA, Al-Thobity AM, Khan SQ, et al. Strength and surface properties of a 3d-printed denture base polymer. J Prosthodont 2022;31:412–8.
[29] Gad MM, Alshehri SZ, Alhamid SA, Albarrak A, Khan SQ, Alshahrani FA, et al. Water sorption, solubility, and translucency of 3d-printed denture base resins. Dent J (Basel) 2022;10.